

1. Introduction

Accelerated electron beams are believed to be responsible for both hard X-ray (HXR) and strong coherent radio emission during solar flares. However, so far the location of the electron acceleration and its physical parameters are poorly known. Solar microwave type III pair burst is possibly the most sensitive signature of the primary energy release and electron accelerations in flares (Aschwanden et al. 1997). A type III pair is composed of two type III burst branches beginning almost at the same time, one is a normal type III burst with negative frequency drift and the other is a reverse-sloped (RS) type III burst with positive frequency drift. The normal branch can track the upward energetic electron beam, and the RS branch is associated to the downward electron beam (Robinson & Benz 2000). In an ideal condition, a type III pair is made up of a normal branch and a RS branch simultaneously (Aschwanden et al. 1993, Huang et al. 1998, Ning et al. 2000). Practically, observations show a group of normal type III bursts at low frequency band and a group of RS type III bursts at higher frequency band occur in same time interval (Aschwanden et al. 1997, Ma et al. 2008, Tan et al. 2016b) which might reflect the complex irregular magnetic structures, repeatedly electron acceleration, and rapid changes in the source regions (Benz et al. 1992, Meshalkina et al. 2004). It is difficult to clarify their one-to-one corresponding relationships. We call this complex assembly a type III pair train.

Microwave type III pairs can be regarded as a sensitive tool to diagnose the physical conditions around the source region of solar bursts where magnetic reconnection, energy release, and particle acceleration take place (Aschwanden & Benz 1997, Sakai et al. 2005, Altyntsev et al. 2007, Mészárosová et al. 2008, Li et al. 2011, Reid, Vilmer, & Kontar, 2011). This work reports a well-observed microwave type III pair train in a solar HXR bursts on 2011 September 26. It is so peculiar that we have never seen so clear microwave type III pair train in impulsive rising phase of the previous solar flares. We apply a recent developed method (Tan et al. 2016a) to derive the physical parameters near the start sites of the above type III bursts. Section 2 presents the observing properties of the microwave type III pair train and the related hard X-ray emission and source information. Section 3 presents the diagnostic results. And finally the conclusion and discussions are summarized in Section 4.

2. Observation of the microwave type III pair train

2.1. Observation of Radio Spectrometer

The microwave type III pair train is observed by the Ondřejov radiospectrograph in the Czech Republic (ORSC). ORSC is an advanced dynamic spectrometer which locates at Ondřejov, the Czech Republic. It receives the solar radio total flux at frequencies of 0.80 - 5.00 GHz with cadence of $\Delta t = 10$ ms and frequency resolution of $\Delta f = 5$ MHz at frequency of 0.80 - 2.00 GHz and $\Delta f = 12$ MHz at frequency of 2.00 - 5.00 GHz (Jiříčka et al. 1993). Figure 1 is the spectrogram of

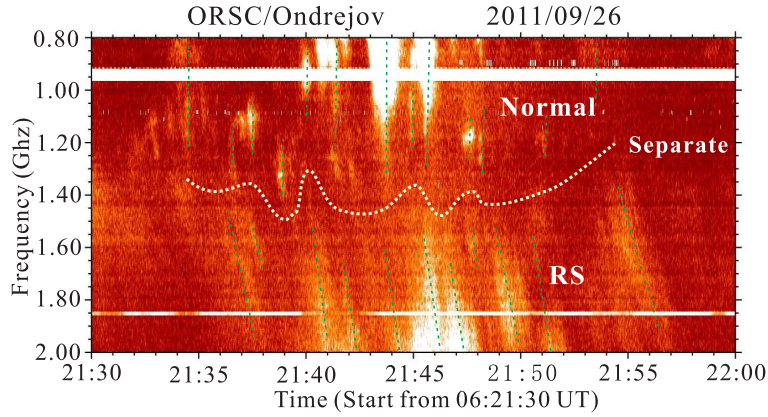


Figure 1. The spectrogram of microwave type III pair train observed by ORSC/Ondřejov on 2011 September 26. Green dashed lines show the ridges of type III bursts. The white dashed curve shows the separate frequency between the normal type III branches and the RS type III branches.

the microwave type III pair train at frequency of 0.80 - 2.00 GHz during 06:21:30 - 06:22:00 UT on 2011 September 26.

The type III pair train is composed of a group normal type III bursts and a group of RS type III bursts. The normal branches start from about 1.30 GHz (start frequency, f_{st} , defined as the frequency at the start point of the microwave type III burst with emission intensity exceeding the background significantly, $> 2\sigma$) and extends below 0.80 GHz with frequency drift defined as the slope of the microwave type III burst on the spectrograms, $D = \frac{df}{dt}$ (f is the emission frequency) in a range of 2.12 - 7.38 GHz s⁻¹ (the relative frequency drift $\bar{D}_n = \frac{df}{f dt} \sim 1.52 - 5.06$ s⁻¹). The RS branches start from about 1.50 GHz and extends beyond 2.00 GHz with frequency drift in a range of 281 - 647 MHz s⁻¹ ($\bar{D}_r \sim 0.23 - 0.50$ s⁻¹). That is to say, the normal branches drift faster than the RS branches by about one order of magnitude. The time difference between the start and end of each type III burst is defined as the burst lifetime (τ). Here, the burst lifetime ranges from 0.14 s to 1.10 s with average of 0.43 s. The whole type III pair train lasts for about 20 s.

From the observation we can see that there is a boundary frequency between the normal and RS type III branches which is defined separate frequency (f_x). For simple type III pair, f_x can be obtained by reverse extending the normal and RS branches and getting a crossing point. The frequency at the crossing point is the separate frequency. For type III pair train, as there is no clear one-to-one relationship between normal and the RS type III branches, f_x can be determined from the frequency at the watershed line between the normal and RS type III group. Usually, f_x is a variable of time. We define $\frac{df_x}{dt}$ as temporal change of separate frequency. The white dotted curve in Figure 1 tracks the variation of the separate frequency (f_x) during the type III pair train. f_x is in a range of 1.225 - 1.494 GHz and has a lumpy variation. There is a frequency gap (δf) between the start frequencies of normal and RS branches, which is in a range of

172 - 442 MHz with average of 277 MHz. Here, the separate frequency is nearly at the middle of the frequency gap (shows in Figure 1).

ORSC observation has no circular polarization record. In the work of Tan et al. (2016b), we made a comparison between the known- and unknown-polarization events and deduced that the emission of the above type III pair train is possibly weak polarization. It is possibly the second harmonic plasma emission (the harmonic number is $s = 2$).

2.2. Hard X-ray Observation

There is no GOES soft X-ray (SXR) observation data during 05:15 - 06:28 UT around the type III pair train. We do not know what SXR flare class of the burst. However, there is a M4.0 flare (start at 05:06 UT, end at 05:13 UT) before and a C4.7 flare (start at 07:28 UT, end at 07:38 UT) after the above type III pair train in active region NOAA 11302 (located at N12E22). At the same time, there are two space telescopes observed a strong HXR burst around the above microwave type III pair train.

One space telescope is the Ramaty High-Energy Solar Spectroscopic Imager (RHESSI). The RHESSI data is processed with the software developed by the RHESSI team (Lin et al. 2002) which have the full-disk flux light curves and the imaging observations. This may help us to determine the temporal evolutionary process of the solar HXR burst associated to the microwave type III pair train and its possible location on the solar disk. Panel (a) of Figure 2 presents the RHESSI HXR light curves in four energy bands (3 - 6, 6 - 12, 12 - 25, 25 - 50 keV). There is a strong HXR burst starting at about 06:18 UT, peaking at about 06:24 UT and ending at about 06:32 UT. The low energy X-ray emission of 3 - 6 keV is relatively smooth with a maximum at about 06:25 UT (black curve in the upper panel). The emission of 6 - 12 keV has some small spikes and reaches to a maximum at about 06:24 UT (red curve in the upper panel). The high energy HXR emission of 12 - 25 keV and 25 - 50 keV have several sharp spikes during 06:21 - 06:24 UT, and one of them occurred during 06:21:30 - 06:22:00 UT (the bottom panel), just covered the above microwave type III pair train (between the two vertical dotted lines).

The other space telescope is the Fermi Gamma-Ray Burst Monitor (GBM, Meegan et al., 2009). GBM is one of the instruments onboard the Fermi Space Telescope (Atwood et al. 2009) launched on June 11, 2008. GBM is specifically designed for observing the whole unocculted sky with a total of 14 scintillation detectors covering the energy range from 8 keV to 40 MeV (Meegan et al. 2009). GBM offers superb capabilities for the analysis of not only γ -ray burst but solar flare HXR burst as well with cadence of about 1 s. Panel (b) of Figure 2 shows the Fermi HXR light curves in the energy bands of 6.1 - 11.4, 12.4 - 24.9, and 26.3 - 49.9 keV, respectively during the above microwave type III pair train. Here, it shows that the microwave type III pairs are closely related to the enhancements of nonthermal HXR emission at energy of 12.4 - 24.9 and 26.3 - 49.9 keV. The low energy X-ray emission (6.1 - 11.4 keV in panel b, and even 3 - 6 keV and 6 - 12 keV in panel a) has poor correlation to the microwave type III pairs.

The radio type III pair train took place just at the impulsive rising phase of the X-ray emission at energy of 3 - 12 keV and coincided with a sharp HXR

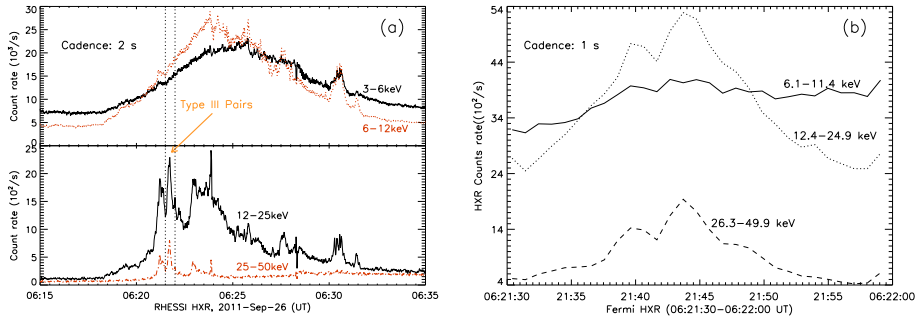


Figure 2. Panel (a): RHESSI HXR light curves in the four energy bands of 3 - 6, 6 - 12, 12 - 25 and 25 - 50 keV in the solar burst on 2011 September 26. The two vertical dotted lines shows the period of microwave type III pair train. Panel (b): Fermi HXR light curves in the energy bands of 6.1 - 11.4, 12.4 - 24.9, and 26.3 - 49.9 keV during the microwave type III pair train.

spike at non-thermal HXR at energy of above 12 keV. These facts imply that the microwave type III pair train is possibly produced by the same population of nonthermal electrons which generated the HXR burst.

2.3. Imaging Observation of the Source Region

There are several telescopes having the imaging observations which may provide the information of the location and structure of the source region of the above HXR burst.

The left panel of Figure 3 presents the contours of HXR intensity observed by RHESSI at energy of 6 - 12 keV (black), 12 - 25 keV (green), and 25 - 50 keV (blue) integrated during 06:18:34 - 06:23:56 UT are overlotted on the magnetogram observed by the Helioseismic and Magnetic Imager onboard the Solar Dynamic Observatory (HMI/SDO) (Scherrer, et al. 2012) at 06:02 UT. HMI observes the vector magnetic field of the full solar disk at 6173\AA with a spatial resolution of about $1''$ and cadence from 90 s to 135 s. Although here AIA/SDO has no imaging observation during 06:05 - 06:28 UT, we may use the above HMI magnetogram to show the main magnetic properties of the source region during the microwave type III pair trains, because generally the magnetic polarity has no obviously change in a time difference of about 20 min. The RHESSI HXR images was reconstructed by using CLEAN algorithm (Hurford et al. 2002, Schwartz et al. 2002). Here we can see that two SXR maxima of 6 - 12 keV overlayed on two regions with same magnetic polarity while two HXR maxima of energy of 12 - 25 keV and 25 - 50 keV are overlaying above the regions with opposite magnetic polarities (P_1 and P_2). It is possible that the HXR maxima of the high energy 25 - 50 keV (P_1 and P_2) are very close to the footpoints of the flaring loop. Their locations are $(-433'', 172'')$ and $(-453'', 114'')$, respectively. The distance between P_1 and P_2 is about $61''$, equals to about 4.4×10^4 km. If we assume the flaring loop is a semicircle and P_1P_2 is the diameter, then the radius is approximated $R_c \sim 2.2 \times 10^4$ km.

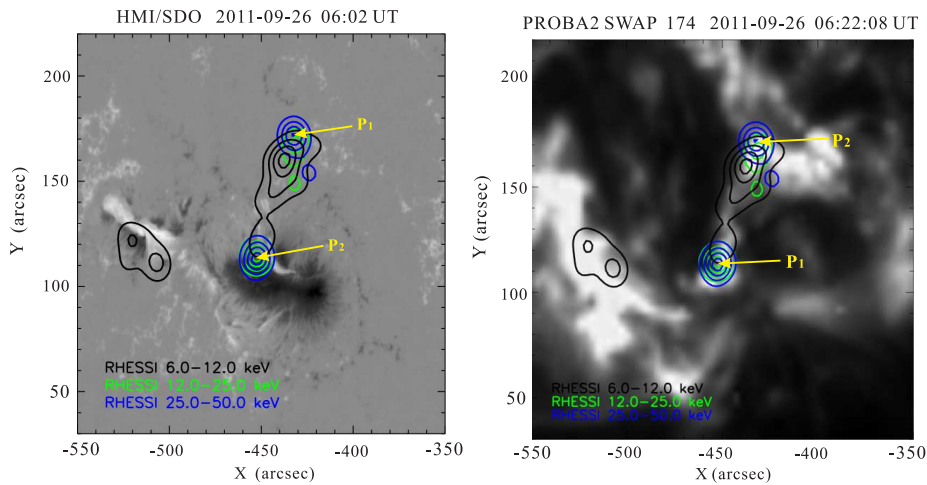


Figure 3. Source region of the solar burst. The background of the left panel is magnetogram observed by HMI/SDO at 06:02 UT while the background of the right panel is a 174 Å EUV image observed by SWAP onboard PROBA-2 at 06:22:08 UT, 2011 September 26. The contours are HXR intensity at energy range of 6 - 12 keV (black), 12 - 25 keV (green), and 25 - 50 keV (blue) observed by RHESSI around the period of the microwave type III pair train. P_1 and P_2 are the footpoint sources with maximum intensities at 25 - 50 keV, respectively.

The background of the right panel in Figure 3 is a 174 Å EUV image observed by a compact solar EUV imaging telescope of the Sun Watcher using APS detectors and image Processing (SWAP) instrument onboard the Project for Onboard Autonomy 2 (PROBA2) satellite at 06:22:08 UT. PROBA-2 is a follow-on ESA micro-satellite technology demonstration mission to the PROBA mission launched on 2011 October 21, and SWAP can obtain one image every minute (Berghmans et al., 2006). The series of SWAP EUV images show a small enhancement near the place of P_2 during the microwave type III pair train. This fact might imply that the downward energetic electron beams associated to the RS type III bursts may contribute to heating the underlying plasmas near the footpoints of the flaring loop.

3. Diagnostics of the Source Region

Now with the above observation evidence we can obtain the physical conditions near the source region of the above solar burst.

3.1. Model and Method

Recently, Tan et al. (2016a) proposed a new set of formulas to diagnose the plasma density (n_e) and magnetic field B near the emission start sites of type III bursts and the velocity of energetic electrons v_i from the observations. As the microwave type III pair train is composed of two branches of microwave type III bursts, it is reasonable to apply them to diagnose the physical conditions near

the source region of primary energy releasing and electron accelerations. Here we modified the schematic diagram of the background conditions of microwave type III pairs in Figure 4. The inflow (the big blue dotted arrows) from the background plasmas (with magnetic field B_0) trigger the magnetic reconnection and particle acceleration in the cusp configuration or in the current sheet above the flaring loops (around C). The upgoing and downgoing energetic electrons (the solid red arrows) produce the plasma emission when they interact with the background plasma. U , D_1 and D_2 are the start sites of the upgoing and downgoing energetic electron beams, respectively. The region between these start sites can be regarded as source region of the solar burst (in the red dotted circle) where magnetic reconnection occurs, electrons can be accelerated to higher energy and the primary energy of the solar burst is released. The distance from the acceleration site (C) to the emission start site of the microwave type III bursts (U , D_1 and D_2) can be regarded as the acceleration length (L_c), it is also the scale size of the source region. Under these assumptions, then plasma density and magnetic fields near the start sites are expressed (Tan et al. 2016a),

$$n_e = f_{st}^2/81s^2 \text{ (m}^{-3}\text{)}, \quad (1)$$

$$B_L < B < B_H \quad (2)$$

$B_L = 3.402 \times 10^{-19}(n_e T \bar{D} R_c)^{\frac{1}{2}}$ and $B_H = 3.293 \times 10^{-16}[\frac{n_e T \bar{D} R_c}{(n_e \tau)^{\frac{1}{3}}}]^{\frac{1}{2}}$ are the lower and upper limits of the magnetic field, respectively. s is the harmonic number, when $s = 1$ is the fundamental plasma emission (always in strong polarization) and $s = 2$ is the second harmonic plasma emission (always in weak polarization). R_c is the curvature radius expressing the divergence of magnetic field lines, T_e is the plasma electron temperature. The average of B_L and B_H can be regarded as the best estimator of magnetic field: $B \sim \frac{1}{2}(B_L + B_H)$.

The velocity of the energetic electrons (v_b) can be approximated (Tan et al. 2016a),

$$v_b \approx \frac{2\mu_0 n_e k_B T}{B^2} \bar{D} R_c, \quad (3)$$

Here, k_B is the Boltzmann constant. Furthermore, the energy of the nonthermal electrons (E in keV) can be derived $E \approx 256 \frac{(v_b/c)^2}{\sqrt{1-(v_b/c)^2}}$, c is the speed of light.

Equation (3) indicates that the beam velocity is dominated not only by the relative frequency drift rate, but also by the magnetic field strength near the emission source region. Here, the velocity is proportional to the relative frequency drift rate, and inverse proportional to the square of magnetic field. This is greatly different from the static barometric model which density scale length only depends on the temperature of the solar medium (Benz et al. 1983). It is also different from the isothermal barometric model which is considering the free-free absorption and the density scale length depends on both of temperature and emission frequency (Dulk 1985, Stahli & Benz 1987).

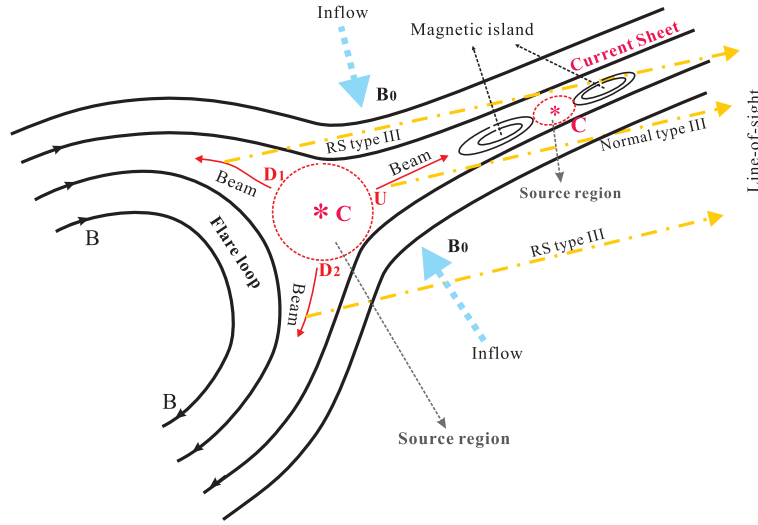


Figure 4. Schematic diagram of the background conditions of microwave type III burst pairs. The red arrows represent the energetic electron beams, the dash-dotted arrows represent the emission propagation. The red D_1 , D_2 and U are the start sites of the RS and normal type III bursts. The red star (C) is the magnetic reconnecting site. The blue arrows reflect the inflows which trigger the magnetic reconnections. The current sheet is located above the flare loop.

With the above results, the plasma β (β_n and β_r) and density scale length (H_n and H_r) near the start sites can be estimated as $\beta = \frac{n_{st} k_B T}{B^2 / (2\mu_0)}$ and $H \approx \frac{1}{2} \beta \cdot R_c$, respectively. Furthermore, the distance between the acceleration and start emission site of the type III bursts can be estimated by,

$$L_c \approx H \cdot \frac{\delta f}{2f_{st}}. \quad (4)$$

As the acceleration distance is related to the frequency difference between the start frequency (f_{st}) and the separate frequency (f_x), which is about a half of the frequency gap (δf). Therefore, there is a factor 2 in the denominator of Equation (4).

As for type III pairs, we can obtain two sets of values associated to the normal and RS branches (f_{stn} , D_n , n_{en} , B_n , H_n , β_n , v_{bn} , E_n , L_{cn}) and (f_{str} , D_r , n_{er} , B_r , H_r , β_r , v_{br} , E_r , L_{cr}). Here, the subscripts n and r are indicated the normal and RS type III branches, respectively. v_{bn} and v_{br} are the velocities of the upgoing and downgoing electron beams while E_n and E_r are their energies, respectively.

Here, it is worth to note that there are two kinds of reconnection sites, one is located in the cusp configuration near the loop top, the other is in the current sheet above the flare loops. As the current sheet may trigger the tearing-mode instability and produce the quasi-periodic pulsating structures in the microwave bursts (Kliem et al. 2000). In this work the type III pair train has no such pulsating property, therefore we tend to suppose the reconnection site is possibly located in the cusp configuration.

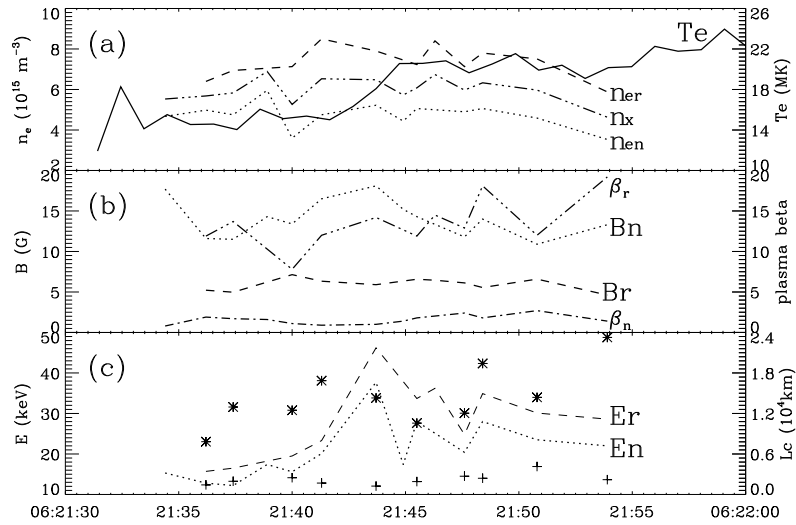


Figure 5. Evolution of the physical conditions around the microwave type III pair train. n_{en} , n_{er} are the plasma density near the start sites of the normal and RS type III branches, respectively. n_x is the plasma density near the acceleration site. T_e is the plasma temperature. B_n and B_r are magnetic field, β_n and β_r are the plasma beta value near start sites of normal and RS type III branches, respectively. E_n and E_r are the energy of the upgoing and downgoing electrons, respectively. The plus (+) and star signs (*) in panel (c) are the acceleration lengths corresponding to the upgoing and downgoing electrons, respectively.

3.2. Diagnostic Results

Using Equation (1) - (4), we may estimate the physical conditions near source region of the solar bursts. Here, the plasma temperature is derived from the X-ray emission observed by GBM/Fermi with cadence of about 1 s (Meegan et al., 2009). The background is subtracted as a values of non-flare periods. The model consists of thermal function (the optically thin thermal bremsstrahlung radiation function for one temperature) and a thick target model in power-law function. The derived temperatures are in a range of 12 - 24 MK during the microwave type III pair train (the black solid curve in panel (a) of Figure 5).

The plasma densities near the emission start sites of the normal and RS type III bursts are over-plotted in dotted and dashed curves in panel (a) of Figure 5, respectively. The density near the start sites of the normal type III bursts is in a range of $(3.5 - 6.0) \times 10^{15} m^{-3}$, and $(5.9 - 8.5) \times 10^{15} m^{-3}$ near the start site of RS type III bursts. We may derive the plasma density near the electron acceleration site (n_x) which is the middle between the above two values, that is around $6 \times 10^{15} m^{-3}$ with little variations (associated to the separate frequency f_x showed by the white solid curve).

The derived magnetic fields near the emission start sites of the type III bursts are showed in panel (b) of Figure 5. It is interesting that the magnetic field near the start site of the RS type III branches is in a range of 4 - 8 Gauss, weaker than that near the start site of the normal type III branches (9 - 18 Gauss). As we know

that RS type III bursts are related to the downgoing electron beams which start site may locate below the acceleration site while the start site of the upward electron beam associated to normal type III bursts is above the acceleration site. Usually, the coronal magnetic field is decreasing with the height which is conflicting with the above results. We may explain this conflict as following: in magnetic reconnection regime, the anti-parallel component of magnetic field near the reconnection site (C) is very close to 0 where is a magnetic singular point and electron acceleration takes place around it (the other place is in the center of current sheet where the magnetic field tends to be near 0). The magnetic field increases from the reconnection site to the emission start sites of microwave type III burst (U , D_1 and D_2), which is obviously different from the general coronal magnetic field.

The velocities of the upgoing energetic electrons are in a range of 0.22 - 0.37 c , a bit smaller than that of the downgoing energetic electrons (0.24 - 0.41 c). The corresponding energies are 12 - 38 keV and 16 - 47 keV for the upward and downward electron beams, respectively (panel (c) of Figure 4). Here, we find that although the RS type III branches drift much slower at about one order of magnitude than the normal type III branches, but the corresponding energy difference of the downgoing and upgoing electrons is only from 2.7 keV to 9.5 keV, which is relatively very small.

Many previous publications show that the energies in both upgoing and downgoing electrons are similar to each other. There is no remarkable difference between the normal and RS type III branches. This is mainly because their relative frequency drift rates of the normal and RS type III branches are similar to each other in their observations (Dulk 1985, Benz et al. 1992, Aschwanden et al. 1995, Meshalkina et al. 2004, etc.). However, in the flare event on 2011-09-26, we found that there is an order of magnitude apart of the relative frequency drift rates between the normal and RS branches. With such great different drift rates, we still obtained similar energies of the upgoing and downgoing electrons. The reason is that although the relative drift rates between the two branches have an order of magnitude apart, but their magnetic field strengths also have several times apart, and these make it is possible to yield similar beam velocities. This can be explained by using Equation (3).

The little difference between the upgoing and downgoing electrons indicates that they may accelerate possibly by the similar mechanism and more effective to the downgoing electrons in the magnetic reconnection region. In the work of Tan et al. (2016b), the same method was applied to the microwave type III pair trains in the postflare phase of an X3.4 flare on 2006 December 13 and found that both of the upgoing and downgoing electrons have almost same energy of 42 - 64 keV.

The small difference of the acceleration in the above two flare events is possibly because the two microwave type III pair events take place in different phase in the solar flares, one is occurred in an impulsive rising phase and the other is in a postflare decay phase. In this work, microwave type III pair train occurs in the impulsive rising phase of the solar HXR burst where the magnetized plasma is possibly much more instable and the magnetic reconnection is stronger. This point can be implied indirectly from the plasma beta (β_p). In this work β_p are

in a ranges of 0.8 - 2.6 and 7.5 - 18.5 in the start sites of the upgoing and downgoing electron beams, respectively. The large value of β_p implies the more violent instability in the magnetized plasma (Drake et al. 2010, Schoeffler et al. 2011). The particle acceleration may be more effective to the downgoing electrons than to the upgoing electrons in the flare impulsive phase. In the X3.4 flare of 2006 December 13, the microwave type III pair trains took place in the postflare decay phase and the β_p in the start site of upgoing electron beams (0.87 - 1.05) was very close to that of the downgoing electron beams (1.09 - 2.74). The little difference of β_p indicates that their magnetic reconnection are at the similar level. Therefore the particle acceleration is also similar to each other.

By using equation (4) we make an estimation of the scale size of acceleration region (L_c) which is in a range of $(1.2 - 4.1) \times 10^3$ km (the plus signs + in panel (c) of Figure 5) for the upgoing electron beams and $(0.8 - 2.3) \times 10^4$ km for the downgoing electron beams (the star sign * in panel (c) of Figure 5). This means that type III bursts begin to generate just after the energetic electron beam propagating a considerable distance from the acceleration site.

4. Summary and Discussions

Using the observations of solar radio spectrometers, hard X-ray emission of RHESSI and Fermi and EUV images of PROBA 2, we diagnosed the physical parameters near the start site of normal and RS type III bursts, which includes the plasma density, temperature, magnetic field, and plasma beta near the start sites of the microwave type III burst, and the primary energy of the upgoing and downgoing electrons and the distance between the acceleration and emission start sites of the type III bursts, respectively. This is the first time to derive so much abundant information of the source region of solar burst directly from the observations. These results present several properties:

(1) The plasma density associated to the start site of RS type III branches is higher than that of normal type III branches, while the magnetic field associated to the emission start site of RS type III branches is weaker than that of normal branches, and these lead to the plasma beta values near the start site of RS type III branches higher than that of the normal branches.

(2) Although the RS type III branches drift slower at about one order of magnitude than the normal type III branches, the energies of the downward electron beams are still very close to that of the upward electron beams.

(3) The plasma density, temperature, magnetic field strength, and the distance between the acceleration and the emission start sites almost have no obvious variations during the period of type III pair trains, while the derived energy of electrons has an obvious peak value which is consistent to the hard X-ray emission during the half minute of type III pair burst.

These facts imply that both of the upgoing and downgoing electron beams are accelerated by similar mechanism in the magnetic reconnection region, and their little difference is just because of their different background conditions, including the plasma density, magnetic field strength and the scale size of the source region, etc.

The above calculations indicate that most of the plasma beta near the emission start sites of microwave type III pair bursts are around or even greatly higher than an unity. This fact may reflect the highly-dynamic properties of the source region where magnetic reconnection and particle accelerations (by the reconnecting electric field) take place. Actually, the magnetic field tends to be very weak and the plasma beta may become very large near the reconnecting site. Around these sites, not only the magnetic reconnection and electron acceleration take place, but also the plasma turbulence and various plasma instabilities occur. Therefore it is much different and complicated from the plasma in the coronal background and flaring loops.

Actually, Equation (2) indicates $B \propto R_c^{1/2}$, and plasma beta value $\beta_p \propto \frac{1}{R_c}$. Figure 4 shows that the upward electron beams may meet the magnetic islands in the current sheet, and here the magnetic curvature radius R_{cn} will possibly become smaller than the radius of the flare loop. We adopt the flare loop to approximate R_c in both normal and RS type III burst regimes, this will overestimate R_c and the magnetic field near the start site of the upward beams, and underestimate the plasma beta. Equation (3) indicates $v_b \propto R_c B^{-2}$ which may derive that the velocity (v_b) is independent to the magnetic field strength. So, the uncertainties of magnetic field will not affect the estimation of the velocity and energy of the electrons.

There are still uncertainties in estimating the magnetic field near the emission start site of the normal type III branches. Equation (2) indicates that magnetic field estimation (B) depends on the curvature radius R_c of the magnetic field lines. R_c for the normal type III branches should be different from that for RS type III branches. Figure 4 shows that the start sites (U) of the upward electron beam locate above the magnetic reconnecting site (C) and the start sites (D_1 and D_2) of downward electron beam locate below the magnetic reconnecting site. D_1 and D_2 are very close to the top of flare loop while U is close to the current sheet above the flare loop. In current sheet, the tearing-mode instabilities may take place and produce magnetic islands and plasmoids which can result in the complex magnetic structures (Kliem et al. 2000). Therefore, the R_c of the magnetic field lines near the site of U may be different to that near D_1 and D_2 . However, so far we have no reasonable method to determine exactly the curvature radius of magnetic field lines near the site of U where the upward electron beams pass through. As an expedient, we simply use the flare loop radius to approximate it. In the near future, it is possible that we can obtain the curvature radius directly from the advanced imaging observation for the normal and RS type III branches, for example the Mingantu Spectral Radiograph (MUSER, the former name is CSRH, Yan et al. 2009).

Acknowledgements The authors are grateful to the referee's kindly and helpful comments for improving this paper. We also thank the ORSC teams in Ondřejov for providing observation data. This work is supported by the NSFC Grants 11273030, 11373039, 11433006, 11573039, and 2014FY120300, CAS XDB09000000, the Grant P209/12/00103 (GA CR) and Project RVO: 67985815 of the Astronomical Institute AS, as well as by the Marie Curie PIRSES-GA-295272-RADIOSUN project.

References

- Altyntsev, A. T., Grechnev, V. V., & Meshalkina, N. S.: 2007, Microwave Type III-Like Bursts as Possible Signatures of Magnetic Reconnection, *Solar Phys.*, 242, 111
- Aschwanden, M. J., Benz, A. O., & Schwartz, R.A.: 1993, The Timing of Electron Beam Signatures in Hard X-Ray and Radio: Solar Flare Observations by BATSE/Compton Gamma-Ray Observatory and PHOENIX, *Astrophys. J.*, 417, 790
- Aschwanden, M. J., & Benz, A. O.: 1995, Chromospheric evaporation and decimetric radio emission in solar flares, *Astrophys. J.*, 438, 997
- Aschwanden, M. J., & Benz, A. O.: 1997, Electron Densities in Solar Flare Loops, Chromospheric Evaporation Upflows, and Acceleration Sites, *Astrophys. J.*, 480, 825
- Atwood, W. B., Abdo, A. A., Ackermann, M., et al.: 2009, Pulsed Gamma Rays from the Millisecond Pulsar J0030+0451 with the Fermi Large Area Telescope, *Astrophys. J.*, 697, 1071
- Benz, A. O., Magun, A., Stehling, W., & Su, H.: 1992, Electron beams in the low corona, *Solar Phys.*, 141, 335
- Berghmans, D., Hochedez, J. F., Defise, J. M., et al.: SWAP onboard PROBA 2, a new EUV imager for solar monitoring, 2006, *Adv. Space Res.*, 38, 1807
- Chen, B., Bastian, T.S., White, S.M., Gary, D. E., Perley, R., Rupen, M. & Carlson, B.: 2013, Tracing Electron Beams in the Sun's Corona with Radio Dynamic Imaging Spectroscopy, *Astrophys. J. Lett.*, 763, 21
- Drake, J.F., Opher, M., & Chamoun, J.N.: 2010, A Magnetic Reconnection Mechanism for the Generation of Anomalous Cosmic Rays, *Astrophys. J.*, 709, 963
- Dulk, G. A.: 1985, Radio emission from the sun and stars, *Ann. Rev. Astron. Astrophys.*, 23, 169
- Fu, Q.J., Ji, H.R., Qin, Z.H., Xu, Z.C., Xia, Z.G., Wu, H.A, et al: 2004, A New Solar Broadband Radio Spectrometer (SBRS) in China, *Solar Phys.* 222, 167
- Huang, G. L., Qin, Z. H., Yan, G., Fu, Q. J., & Liu, Y. Y.: 1998, The Energetic Spectrum of Non-Thermal Electrons in an Acceleration Region Calculated From a Solar Microwave Type III Burst with both Positive and Negative Frequency Drifts, *Astrophys. Space Sci.*, 259, 317
- Jiříčka, K., Karlický, M., Kepka, O., & Tlamicha, A.: 1993, Fast drift burst observations with the new Ondrejov radiospectrograph, *Solar Phys.*, 147, 203
- Karlický, M.: 2014, Solar flares: radio and X-ray signatures of magnetic reconnection processes, *Res. Astron. Astrophys.*, 14, 753
- Kliem, B., Karlický, M., & Benz, A. O.: 2000, Solar flare radio pulsations as a signature of dynamic magnetic reconnection, *Astron. Astrophys.*, 360, 715
- Li, B., Cairns, I.H., Yan, Y.H., & Robinson, P.A.: 2011, Decimetric Type III Bursts: Generation and Propagation, *Astrophys. J. Lett.*, 738, 9
- Lin, R. P., Dennis, B. R., Hurford, G. J., et al.: 2002, The Reuven Ramaty High-Energy Solar Spectroscopic Imager (RHESSI), *Solar Phys.*, 210, 3
- Meegan, C.; Lichti, G., Bhat, P. N., et al.: 2009, The Fermi Gamma-ray Burst Monitor, *Astrophys. J.*, 702, 791
- Meshalkina, N. S., Altyntsev, A.T., Sych, R.A., Chernov, G.P., & Yan, Y.H.: 2004, On the wave mode of subsecond pulses in the cm-range, *Solar Phys.*, 221, 85
- Mészárosová, H., Karlický, M., Sawant, H.S., et al.: 2008, Solar decimetric type III bursts in semi-closed magnetic field structures, *Astron. Astrophys.*, 484, 529
- Ning, Z. J., Fu, Q. J., & Lu, Q. K.: 2000, Type III burst pair, *Solar Phys.*, 194, 137
- Reid, H. A. S., Vilmer, N., & Kontar, E. P.: 2011, Characteristics of the flare acceleration region derived from simultaneous hard X-ray and radio observations, *Astron. Astrophys.*, 529, A66
- Robinson, P. A., & Benz, A. O.: 2000, Bidirectional Type III Solar Radio Bursts, *Solar Phys.*, 194, 345
- Sakai, J. I., Kitamoto, T., Saito, S.: 2005, Simulation of Solar Type III Radio Bursts from a Magnetic Reconnection Region, *Astrophys. J.*, 622, 157
- Scherrer, P.H., Schou, J., Bush, R.I., Kosovichev, A.G., Bogart, R.S., Hoeksema, J.T., et al.: 2012, The Helioseismic and Magnetic Imager (HMI) Investigation for the Solar Dynamics Observatory (SDO), *Solar Phys.*, 210, 165
- Schoeffler, K.M., Drake, J.F., Swisdak, M.: 2011, The Effects of Plasma Beta and Anisotropy Instabilities on the Dynamics of Reconnecting Magnetic Fields in the Heliosheath, *Astrophys. J.*, 743, 70

-
- Schwartz, R. A., Csillaghy, A., Tolbert, A. K., Hurford, G. J., McTiernan, J., Zarro, D.: 2002, RHESSI Data Analysis Software: Rationale and Methods, *Solar Phys.*, 210, 165
- Stahli, M., Benz, A. O.: 1987, Microwave emission of solar electron beams, *Astron. Astrophys.*, 175, 271
- Tan, B. L., Karlický, M., Mészárosóvá, H., & Huang, G.L.: 2016a, Diagnosing physical conditions near the flare energy-release sites from observations of solar microwave type III bursts, *Res. Astron. Astrophys.*, 16, 82
- Tan, B. L., Mészárosóvá, H., Karlický, M., Huang, G.L., & Tan, C.M.: 2016b, Microwave Type III Pair Bursts in Solar Flares, *Astrophys. J.*, 819, 42
- Thomas R.J., Starr R., & Crannell C.J., 1985, Expressions to determine temperatures and emission measures for solar X-ray events from GOES measurements, *Solar Phys.*, 95, 323
- Yan, Y.H., Zhang, J., & Wang, W., et al. 2009, The Chinese Spectral Radioheliograph CSRH, *Earth Moon & Planet*, 104, 97